DRA/GODDARD

FINAL REPORT

NASA Contract NAS5-22929

covering the period

February 1, 1976 - April 30, 1984

submitted by:

D. H. Staelin (principal investigator),
W. T. Baumann, T. S. Bigelow,
P. W. Rosenkranz, Xu Xi-ru

June 15, 1984

Research Laboratory of Electronics
Massachusetts Institute of Technology
Cambridge, Massachusetts 02139

Introduction

The research supported by this contract was directed toward inversion and interpretation of data produced by the Nimbus-7 Scanning Multichannel Microwave Radiometer (SMMR). There were five principal subjects: 1) modeling of the emissivity of foam patches on the ocean surface; 2) inversion of radiometric data by a multidimensional algorithm; 3) an operational water vapor retrieval algorithm; 4) inference of Antarctic firn accumulation rates; 5) inference of water vapor over the Arctic sea ice.

1. Ocean foam emissivity

Foam on the ocean was modeled as a dielectric slab with a dielectric constant which varied with height above the ocean surface. An example of these computations is given in figure 1, which plots emissivity at 37 GHz vertical and horizontal polarization as a function of incidence angle, with foam thickness as a parameter. Curves for 0, .5 and 2 cm thickness are shown. This computation assumed a flat surface under the foam. The emissivity of a surface roughened by depressions due to floating bubbles was also computed, and is plotted in figure 2, at 37 and 19 GHz. Three curves are shown for each polarization; two computations for rms roughness of .026 and .1 cm, and measurements of foam reported by Stogryn (1972). The angular variation of the calculations for .1 cm is similar to the measurements, suggesting that small-scale roughness is important. This work is described in an M.S. thesis by Bigelow (abstract appended).

2. Multidimensional inversion

In the case of SMMR, the data has three dimensions: scan number (varies with distance parallel to the satellite track), distance along a scan, and channel number (or

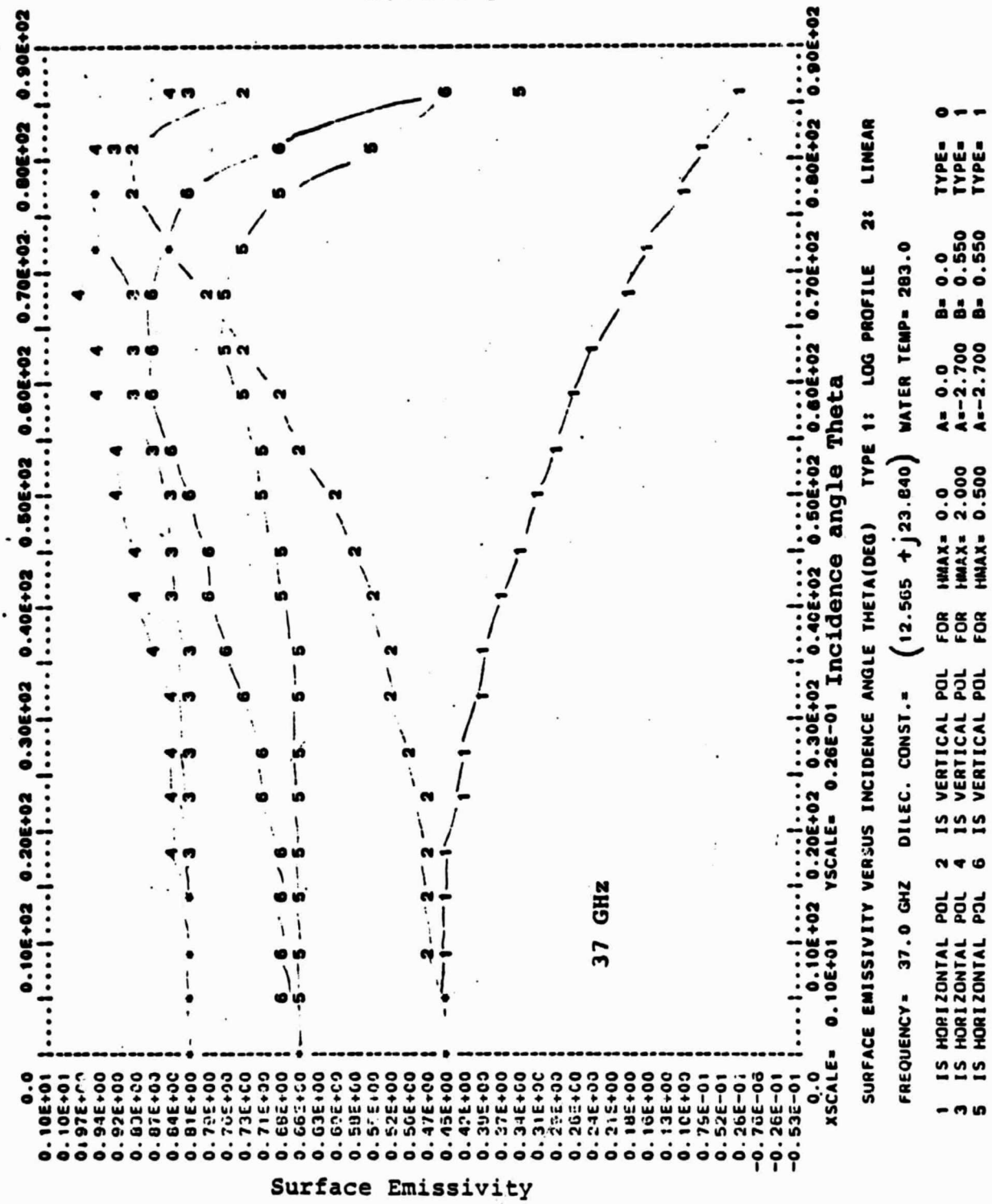

Figure 1 Calculated surface emissivity vs. incidence angle for 100% foam cover for parameters indicated.

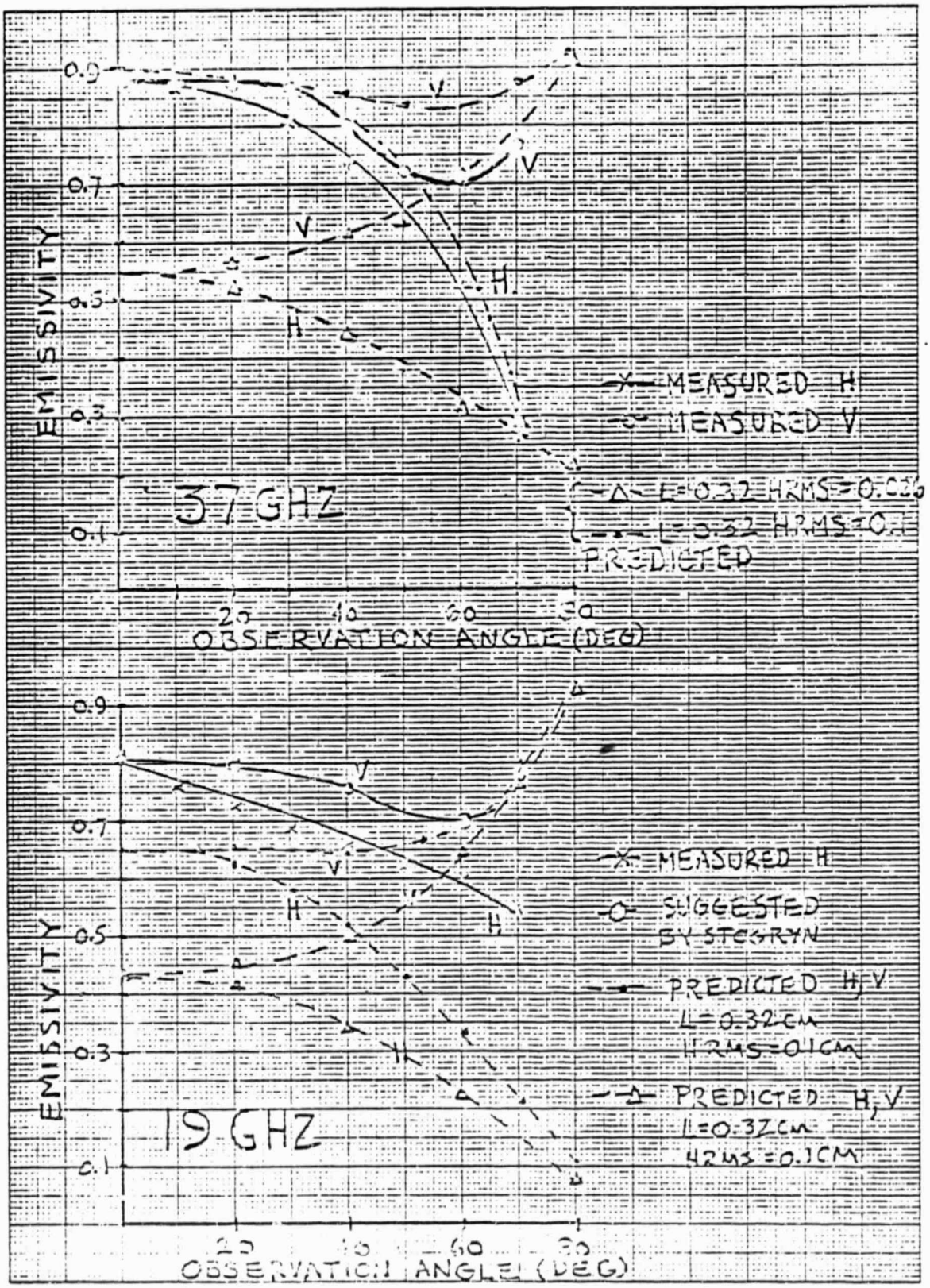

Figure 2 Comparison of calculated emissivity with surface Roughness and Stogryn's reported measurements at 19 and 37 GHz.

frequency and polarization). The antenna beam width is approximately proportional to wavelength. In the operational SMMR data processing, brightness temperatures for each channel are binned at resolutions comparable to or larger than the beamwidth. As a result, longer wavelength brightness temperatures are not available at the desired resolution of some of the geophysical parameters, to be used in estimating them. This circumstance motivated work on a new retrieval algorithm. Our solution was to do the inversion in the spatial Fourier transform domain. This approach allowed the combination of data from all channels of the instrument to estimate each parameter; furthermore, spatial correlations of the geophysical parameters and the antenna gain pattern were accounted for. This algorithm is described in a series of papers by Rosenkranz and Baumann (1980) and Rosenkranz (1981-82) (abstracts are appended).

These advantages of a multidimensional algorithm were expected to be most significant in situations where the structure of weather patterns was highly developed -- for example, in tropical storms. Unfortunately, because of the typically very heavy precipitation in these storms, the inversion problem is very nonlinear. Figure 3 and table 1 compare estimates of maximum wind speed made by the multidimensional algorithm operating on SMMR data with estimates from observers, for several tropical storms. There is some correlation, except for the two storms Tess and Faye (points 2, 3 and 5), although the variability is underestimated.

3. Operational water vapor algorithm

For operational use, MIT supplied to GSFC an algorithm for estimation of water vapor from the 18, 21 and 37 GHz SMMR brightness temperatures. The estimate is of the form

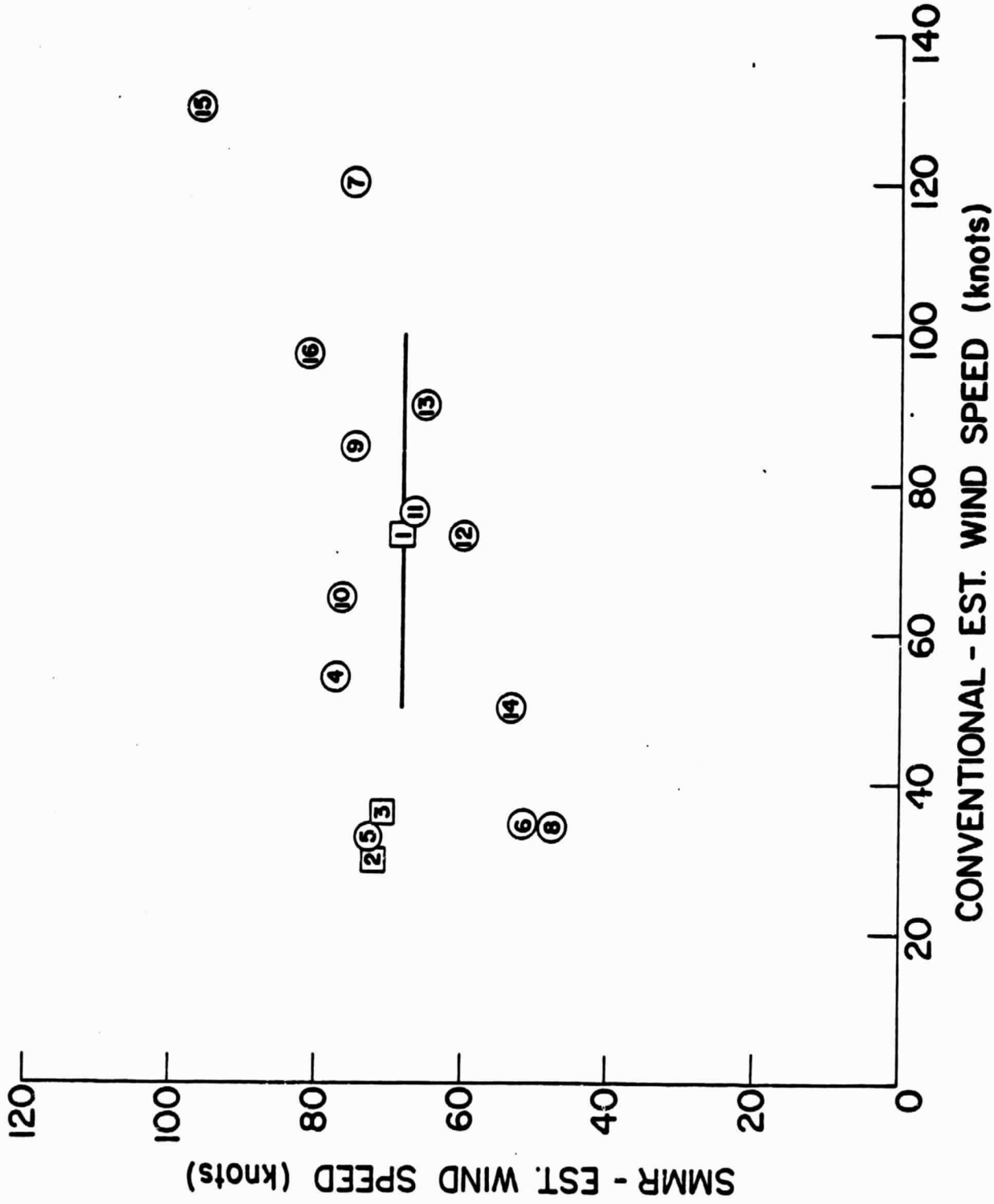

Figure 3. Comparison of SMMR-derived and conventional estimates of maximum wind speed in tropical storms.

Table 1. Key to Figure 3.

STORM		TIME AND DATE OF SMMR OBSERVATION	
1)	KENDRA	1618Z	30 OCT. 78
2)	TESS	1403Z	1 NOV. 78
3)	TESS	1421Z	2 NOV. 78
4)	TC-21-78	1811Z	21 NOV. 78
5)	FAYE	0258Z	5 JUL. 79
6)	DOLORES	1854Z	17 JUL. 79
7)	DOLORES	1932Z	19 JUL. 79
8)	DAVID	0243Z	26 AUG. 79
9)	DAVID	0358Z	30 AUG. 79
10)	FREDERIC	0253Z	1 SEPT. 79
11)	LOLA	0143Z	5 SEPT. 79
12)	OWEN	0247Z	25 SEPT. 79
13)	OWEN	1536Z	25 SEPT. 79
14)	ROGER	1517Z	5 OCT. 79
15)	TIP	0236Z	11 OCT. 79
16)	TIP	0248Z	17 OCT. 79

$$\hat{V} = V_o + aV^* + b(V^*)^2$$

where

$$V^* = \sum_i d_i (T_{Bi} - T_{oi})$$

and V_o, a, b, d_i, T_{oi} are constant coefficients. After tuning of the coefficients a and b at GSFC, retrievals agreed with radiosonde measurements to an rms accuracy of 1 precip. mm.

4. Antarctic firn accumulation rates

A study of the brightness temperatures measured by SMMR over the Antarctic firn showed that they could be related to snow accumulation rate, given in situ measurements from a small number of bore sites and surface temperatures. This work is described in an unpublished manuscript by Staelin and Xu.

5. Arctic water vapor

The brightness temperature spectrum of the Arctic sea ice varies with age, temperature and other factors. It was observed, however, that the brightness temperature at 21 GHz departed from a smooth curve drawn through the other frequencies. This spectral feature was attributed to atmospheric water vapor and the SMMR brightness temperatures were used to map water vapor over the ice. These maps showed increases in water vapor in the vicinity of large polynyas.